4596 *Biochemistry* **2009,** *48,* 4596–4606
DOI:10.1021/bi9003342

BIOCHEMISTRY
including biophysical chemistry & molecular biology
Article

Solution Structure and Dynamics of ERp18, a Small Endoplasmic Reticulum Resident Oxidoreductase[†,‡]

Michelle L. Rowe,[§] Lloyd W. Ruddock,[∥] Geoff Kelly,[⊥] Jürgen M. Schmidt,[§] Richard A. Williamson,*[,§] and Mark J. Howard*[,§]

[§]*Department of Biosciences, University of Kent, Canterbury, Kent CT2 7NJ, United Kingdom,* [∥]*Department of Biochemisty, University of Oulu, P.O. Box 3000, Oulu FIN-90014, Finland, and* [⊥]*The National Institute for Medical Research, The Ridgeway, Mill Hill, London NW7 1AA, United Kingdom*

Received February 26, 2009; Revised Manuscript Received April 9, 2009

ABSTRACT: Here we report the solution structure of oxidized ERp18 as determined using NMR spectroscopy. ERp18 is the smallest member of the protein disulfide isomerase (PDI) family of proteins to contain a Cys-Xxx-Xxx-Cys active site motif. It is an 18 kDa endoplasmic reticulum resident protein with unknown function although sequence similarity to individual domains of the thiol−disulfide oxidoreductase PDI suggests ERp18 may have a similar structure and function. Like the catalytic domains of PDI, ERp18 adopts a thioredoxin fold with a thioredoxin-like active site located at the N-terminus of a long kinked helix that spans the length of the protein. Comparison of backbone chemical shifts for oxidized and reduced ERp18 shows the majority of residues possess the same backbone conformation in both states, with differences limited to the active site and regions in close proximity. S^2 order parameters from NMR backbone dynamics were found to be 0.81 for oxidized and 0.91 for reduced ERp18, and these observations, in combination with amide hydrogen exchange rates, imply a more rigid and compact backbone for the reduced structure. These observations support a putative role for ERp18 within the cell as an oxidase, introducing disulfide bonds to substrate proteins, providing structural confirmation of ERp18's role as a thiol−disulfide oxidoreductase.

A great many proteins essential for life contain one or more intramolecular disulfide bonds. These disulfide bonds help to stabilize the protein and in some cases are important for their functionality. During formation of these disulfide bonds it is important for the correct cysteine residues to be paired together in order to achieve the correct three-dimensional (3D) structure. Within the endoplasmic reticulum (ER) there are a number of proteins that are thought to help in the formation (oxidation), breakage (reduction), and isomerization of disulfide bonds so that the correct fold can be achieved (*1*, *2*). These reactions are all catalyzed by members of the thioredoxin superfamily, each having at least one thioredoxin-like domain and a thioredoxin-like active site motif of the form Cys-Xxx-Xxx-Cys. Members of the human PDI family of proteins, for which the three-dimensional structures have been determined, show at least one domain that displays a thioredoxin-like fold with a central mixed β-sheet surrounded by helices. Apart from displaying a similar fold, domains within members of the PDI family share several other conserved features suggesting that these features are important for the function of such proteins.

(i) The Cys-Xxx-Xxx-Cys active site motif of thioredoxin related proteins is always located on a turn immediately before helix 2, with the C-terminal active site cysteine being part of helix 2.

The active site motif can vary between members of the family, and this can be used as an indication of function. For example, family members with a Cys-Gly-Pro-Cys active site, as seen in thioredoxin itself, are generally disulfide reductants whereas DsbA, a highly oxidizing PDI-related protein found in *Escherichia coli*, has the active site motif Cys-Pro-His-Cys. Many PDI family members have multiple Cys-Gly-His-Cys active sites and also inactive thioredoxin domains, and these have both thiol−disulfide oxidase and isomerase activity. However, some members of the PDI family have one or more of the cysteine residues in this motif replaced by serine and therefore lack the disulfide oxidoreductase activity of other family members.

(ii) Thioredoxin folds often contain a conserved *cis*-proline residue located in the turn before strand 4. This is located in the vicinity of the active site of catalytic domains. The purpose of this *cis*-proline is not known, but it may be implicated in substrate binding. Removal of the *cis*-peptide bond by mutation to alanine gives rise to a significant conformational change in DsbA (*3*), and equivalent mutations in the **a** and **a**′ domains of yeast PDI lead to abolition of refolding activity (*4*).

[†]The authors thank the BBSRC for a studentship to M.L.R. This work was also supported by BBSRC Project Grants 96/B17912 and BB/D017807/1.

[‡]Chemical shifts and coordinates of oxidized ERp18 have been deposited in the Biological Magnetic Resonance Bank (accession number 15964) and Protein Data Bank (accession number 2K8V), respectively. The backbone chemical shifts for reduced ERp18 have also been deposited in the Biological Magnetic Resonance Bank under accession number 7430.

*To whom correspondence should be addressed. M.J.H.: E-mail: m.j.howard@kent.ac.uk. phone: +44 1227 824730. fax: +44 1227 763912. R.A.W.: E-mail: r.a.williamson@kent.ac.uk. phone: +44 1227 827155. fax: +44 1227 763912.

 Published on Web 4/10/2009

(iii) A further conserved proline is found in the α-helix immediately following the active site that causes this helix to bend and disrupts the secondary structure. This proline is not present in the new human family members AGR2 and AGR3, referred to as Hag2 and Hag3 by Appenzeller-Herzog and Ellgaard (*1*), or in Mpd1p from *Saccharomyces cerevisiae* (*5*).

(iv) A buried charge pair, Glu30 and Lys64 in PDI **a** (*6*), located in proximity to the active site, that may be involved in proton transfer reactions important for the stability and mechanism of PDI, as per Asp27 and Lys57 in *E. coli* thioredoxin (*7*, *8*).

(v) A conserved arginine residue, Arg120 in the PDI **a** domain, is thought to modulate the pK_a of the active site cysteines (*9*) and is implicated in the reoxidation of PDI and the release of the substrate.

This study focuses on the ER resident protein ERp18 (*10*), the smallest member of the PDI family to have a Cys-Xxx-Xxx-Cys active site motif. ERp18 contains the unusual Cys-Gly-Ala-Cys active site sequence, and so its function could differ from that of the molecules described above. ERp18 has been investigated by several groups under different names: ERp19 (*11*), hTLP19 (*12*), and more recently ERp16 (*13*). Investigation into the function of ERp18 is limited, but cellular location and activity assays have given some insight into its physiological role. Sequence analysis shows that ERp18 contains a putative endoplasmic reticulum localization motif, EDEL, similar to the KDEL found in many other ER resident proteins and has been shown to be located within the ER by several independent groups (*10*, *11*, *13*). ERp18 has been shown to have 15−20% of the oxidase activity of PDI (*10*, *13*) and has been reported to have 22% of the PDI isomerase activity (*13*). ERp18 has been found to play an important role in cellular defense against prolonged ER stress, and its redox potential and inhibition of dithiothreitol (DTT) induced apoptosis suggest that ERp18 contributes to disulfide bond formation in nascent proteins (*13*).

Here we provide confirmation of function via the elucidation of the solution structure and analysis of backbone dynamics using nuclear magnetic resonance (NMR) spectroscopy. ERp18 exhibits a thioredoxin fold consisting of a four-stranded β-sheet surrounded by four helices, yet has several unusual features previously thought to be conserved among PDI family members.

Full resonance assignment has been completed for the oxidized form of ERp18 as well as extensive backbone resonance assignment of the reduced form of ERp18 using a range of heteronuclear, multidimensional NMR experiments. Through-space NMR experiments were used to obtain structural information of oxidized ERp18, and solution structure ensembles were calculated using the crystallography and NMR system (CNS). Backbone assignments and HSQC experiments of the reduced form of ERp18 allowed comparative NMR dynamics and amide hydrogen exchange rates for oxidized versus reduced ERp18 to be collected. The results of these investigations and the impact on the potential function of ERp18 are discussed.

EXPERIMENTAL PROCEDURES

Protein Expression and Purification. ERp18 was expressed in *E. coli* BL21(DE3) pLysS strain with an N-terminal His tag and purified as described previously (*10*). Isotopic labeling with ^{13}C and ^{15}N was achieved by expression of ERp18 in M9 medium enriched with [^{13}C]glucose and [^{15}N]ammonium sulfate.

Multidimensional NMR Spectroscopy. Oxidized and reduced ERp18 samples were prepared by incubation for 30 min at room temperature with a 4-fold molar excess of oxidized glutathione or a 10-fold molar excess of dithiothreitol, respectively. Glutathione was removed from oxidized samples by buffer exchange prior to NMR experiments whereas dithiothreitol remained to prevent reoxidation. The oxidation state of the protein was confirmed by the appearance of the ^{15}N-HSQC (see Figure 1) and was checked before and after any series of experiments. ERp18 samples used for NMR experiments were 0.5 mM for relaxation experiments and 1 mM for structural experiments. All samples were prepared in 20 mM sodium phosphate and 100 mM sodium chloride, pH 6.5. Sample volumes of 330 μL were placed in Shigemi BMS-005V tubes and included 10% D_2O. All NMR experiments were carried out at 600 MHz using a Varian Unity INOVA equipped with a 5 mm HCN *z*-pulse field gradient probe except heteronuclear NOESY spectra that were recorded at 800 MHz using a Varian Unity INOVA spectrometer at NIMR, Mill Hill. Chemical shift referencing was based on the position of the water resonance with the exact value being related to the known relationship of the ^1H_2O resonance with temperature (*14*). Unless otherwise stated, all NMR experiments were solvent suppressed to reduce the water signal using WATERGATE (*15*) that was typically obtained using a gradient field strength of 40−50 G cm^{-1}. All indirect NMR dimensions were acquired using the hypercomplex method (*16*), and all reported data numbers reflect the total of real and imaginary points collected in each dimension. Experiments were carried out at 25 °C, and an additional ^{15}N-edited TOCSY experiment was carried out at 35 °C to optimize signal transfer. All NMR data processing was carried out using NMRPipe (*17*), chemical shifts were assigned using NMRView (*18*, *19*), and manual NOE assignment was carried out using the CCPN analysis package (*20*, *21*).

NMR Resonance Assignment. Backbone chemical shift assignment was achieved using $^1H-^{15}N$ HSQC, CBCANH, CBCA(CO)NH, HBHA(CBCA)NH, HBHA(CBCACO)NH, C(CO)NH, and HNCO experiments; side chain assignments were achieved using HCCH-TOCSY, ^{15}N-edited TOCSY, $^1H-^{13}C$ HSQC, and where necessary ^{15}N-edited NOESY and ^{13}C-edited NOESY experiments. Chemical shift differences between the backbone amide ^{15}N and ^1H resonances of oxidized versus reduced ERp18 were calculated using the equation:

$$\text{shift difference} = \sqrt{(\Delta^1\text{H})^2 + \frac{1}{6}(\Delta^{15}\text{N})^2}$$

where Δ^1H and $\Delta^{15}N$ are the chemical shift values (in ppm) of amide proton and nitrogen, respectively. The nitrogen value is weighted to account for the larger range of ppm values in this dimension.

Structural Calculations of Oxidized ERp18. NOE distance restraints were manually assigned from ^{15}N-edited NOESY and ^{13}C-edited NOESY spectra using CCPN analysis. Structural calculations were performed using CNS (*22*) and refined by inclusion of dihedral angles predicted from backbone chemical shifts using TALOS (*23*) and hydrogen bonds determined from hydrogen exchange experiments and visual analysis of structure outputs. The CISP patch was used in the CNS input in order to define the conserved proline residue as being in the *cis* conformation as defined from Cβ chemical shifts. During the simulated annealing protocol of CNS for the final ensemble, calculations were performed with 10000 cooling steps from 50000 to 2000 K similar to previously reported methods (*24*).

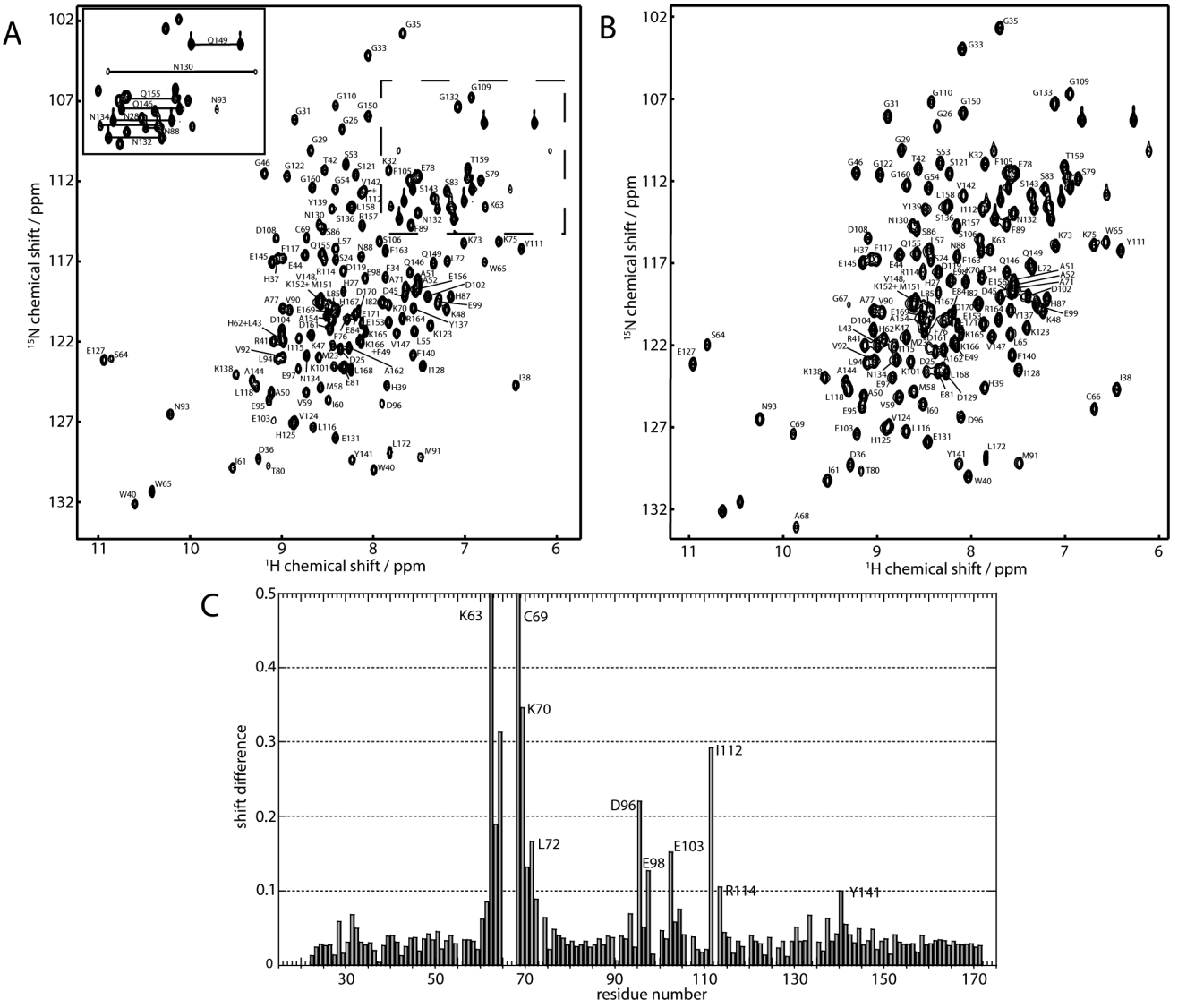

FIGURE 1: ^{1}H−^{15}N HSQC spectra of oxidized (A) and reduced (B) ERp18. Assignments for some of the backbone cross-peaks are shown using one-letter amino acid code and sequence number. The difference in backbone ^{15}N−^{1}H chemical shift for each residue is shown in the chemical shift map (C) with residues that are seen to change significantly labeled. Note that residues C66, G67, and A68 are only seen in the reduced spectrum.

^{15}N Relaxation Measurements. ^{15}N T_1 and T_2 experiments were acquired using well-developed pulse sequences similar to those described elsewhere (*25*). T_1 and T_2 delay times were set as 128, 256 (×2), 384, 512, 640 (×2), 769, and 897 ms and 20, 40, 60 (×2), 80, 100, 120 (×2), 140, and 160 ms, respectively. ^{15}N heteronuclear NOE experiments were collected with a relaxation delay of 5 s with and without saturation of the amide protons. Saturation was achieved using 120° high-power pulses (*26*), and spectra were collected with 2048 points (9000 Hz) in F_2 and 192 points (2100 Hz) in F_1. Relaxation times were calculated as the exponential fit of single exponential decays to peak intensity values: $I = I_0 \exp(-t/T_x)$, where $T_x = T_1$ or T_2 and I = resonance intensity at time t. Heteronuclear NOEs were calculated according to the Noggle and Schirmer definition of $(I - I_0)/I_0$ (*27*) except for model-free analysis where I/I_0 was used. Model-free analysis of the relaxation data was carried out using the ModelFree 4.0 suite of programs (*28*−*30*) to obtain the simplest fits (one or two parameter) of S^2 (order parameter of motion) and R_{ex} (exchange broadening) for reduced and oxidized ERp18, respectively.

^{15}N−^{1}H Hydrogen Exchange. Slow exchanging amide protons were identified from rapidly acquired ^{15}N−^{1}H HSQC experiments taken from lyophilized oxidized and reduced ERp18 resuspended in 100% D_2O. Each experiment was acquired with 2048 points in the direct dimension and 128 points in the indirect dimension and took 300 s to complete. Experiments were collected over 3 h for both oxidized and reduced ERp18. The decay in resonance volume was fitted to a monoexponential decay, as in ^{15}N relaxation data, to the equation $I = I_0 \exp(-kt)$, where I is the intensity at time t defined by an exponential decay with decay constant k.

RESULTS

Protein Expression and Purification. ^{15}N and ^{13}C/^{15}N isotopically labeled ERp18 were recombinantly expressed with an N-terminal His tag using *E. coli* BL21(DE3) pLysS cells with yields of up to 60 mg/L. Purification using metal affinity chromatography followed by anion-exchange chromatography produced ERp18 with a purity level greater than 95% as determined by SDS−PAGE and mass spectrometry.

Chemical Shift Assignments. Backbone chemical shift assignments were completed for both oxidized and reduced forms of ERp18, with 98%, 99%, and 99% assignment, respectively, for backbone amide, C_α, and C_β resonances for oxidized ERp18 and 100%, 100%, and 99% for reduced. No assignments could be made for the Cys-Gly-Ala residues of the active site for the oxidized protein in the $^1H-^{15}N$ HSQC. Comparison of the chemical shifts of proline residues with random coil chemical shift values for proline residues in both the *cis* and *trans* conformation (*31*) reveals that proline-113 is in the *cis* conformation, based on the higher chemical shift value for the C_β nucleus.

The $^1H-^{15}N$ HSQC spectra in Figure 1 show assigned amide resonances for oxidized (A) and reduced (B) ERp18. The differences in chemical shift between these two forms can be seen in the chemical shift map (C) that shows the majority of resonances do not significantly change with oxidation state; however, some resonances appear at different chemical shifts for each form of the protein, particularly in the immediate vicinity of the active site Cys-Xxx-Xxx-Cys motif. TALOS analysis of backbone chemical shifts from ERp18 confirmed that the definition and limits of secondary structure were the same for both oxidized and reduced protein. Side chain assignments were completed for oxidized ERp18 to allow structure calculations of this form of the protein.

Structure Calculations. Structural calculations were performed using a combination of manually assigned NOE data, dihedral angles, and hydrogen bond information. The use of the CISP patch to define the *cis* conformation of proline-113 produced a structure with lower energy than that with Pro113 in the *trans* conformation, as calculated using GROMOS96 43B1 parameter set (*32*) within DEEPVIEW version 3.7 (*33*). Table 1 summarizes the statistics for the 40 structure ensemble shown in Figure 2A including the results of PROCHECK-NMR (*34*) analysis of the ensemble. The use of 10000 cooling steps in the simulated annealing of ERp18 structure calculation gave an improved RMSD for the calculated ensemble compared to calculations performed with the standard 1000 cooling steps (data not shown).

Tertiary Structure of Oxidized ERp18. The final structure ensemble shows ERp18 to display a thioredoxin-like fold consisting of a central four-stranded β-sheet surrounded by four helical sections as seen in Figure 2. Figure 2D shows the secondary structure pattern and limits as indicated by the residue numbers underneath the scheme. Figure 2B shows the strands in the order (left to right) $\beta2$-$\beta1$-$\beta3$-$\beta4$ with $\beta3$ being antiparallel to the other strands. Helix 2 is subdivided into three helical sections with a 3_{10}-helical section between two α-helices as determined from NOE connectivites, dihedral angles, and hydrogen-bonding patterns. This manifests as a bend in the helix and allows it to span from one end of the β-sheet to the other. Helix 3 is also a 3_{10}-helix from the pattern of NOE connectivities. Three-dimensional structure comparison using DaliLite v.3 (*35*) revealed structural similarity of ERp18 to many thioredoxin fold proteins; the top 50 structural matches featured thioredoxins from many plant and animal species. These included the first thioredoxin domain of mouse PDI (2DML, unpublished) and the C-terminal domain of DsbD, a bacterial oxidoreductase (*36*). Also within the top 50 matches were molecules that are not PDI related: Fas-associated factor 1 (2EC4, unpublished), spliceosomal U5 snRNP-specific 15 kDa protein (*37*), and the UAS domain of UBX-domain-containing protein 7 (2DLX, unpublished). Unsurprisingly, the closest match was with that of Rp19, a crystal structure of ERp18 with the PDB accession code of 1SEN (unpublished).

Table 1: Structural Statistics for the 40 Structure Ensemble of Oxidized ERp18

parameter	value
No. of NOE Restraints	
total	2979
intraresidue	1621
sequential	642
medium range	358
long range	358
hydrogen bonds (Å)	52
dihedral angles (deg)	153
NOE violations > 0.2 Å	0
dihedral angle violations > 2.0°	0
Lennard-Jones energy (kJ mol^{-1})	−3183.1
RMSD Backbone (C′, Cα, N) (Å)	
residues 20−145	0.846
residues in secondary structure	0.678
RMSD Heavy Atoms (Å)	
residues 20−145	1.386
residues in secondary structure	1.169
Ramachandran Plot (%)	
most favored regions	64.4
additionally allowed regions	26.9
generously allowed regions	6.0
disallowed regions	2.8

Backbone Dynamics. In order to probe the dynamic behavior of the two oxidation states of ERp18 and how this relates to function, measurements of ^{15}N longitudinal and transverse (T_1 and T_2) relaxation times and $^{15}N-^1H$ heteronuclear NOEs were measured. Plots of each of these parameters against residue number can be found in the Supporting Information. The mean ^{15}N T_1 values over the structured regions of the protein (those within 1 standard deviation of the mean) for oxidized and reduced thioredoxin were 732 ± 40 and 706 ± 30 ms, respectively. The mean T_2 values were 88 ± 16 ms for oxidized ERp18 and 99 ± 9 ms for reduced ERp18; this gave T_1/T_2 ratios of 8.32 and 7.13 for oxidized and reduced ERp18, respectively.

The values for hetNOE and R_1 ($1/T_1$) and R_2 ($1/T_2$) were used for model-free analysis (*28*, *29*). The results of model-free calculations are shown in Figure 3 for both oxidized and reduced ERp18. The order parameter S^2 is plotted against residue number for both oxidized and reduced ERp18, and where needed R_{ex} values were also plotted. No R_{ex} values were required to fit reduced ERp18 NMR relaxation data. Both oxidized and reduced ERp18 show similar patterns with decreased S^2 values seen for loop regions, in particular, the loop containing the 3_{10}-helix, helix 3, and the loop preceding helix 4. The mean and standard deviation of S^2 was calculated to be 0.81 ± 0.11 and 0.91 ± 0.1 for oxidized and reduced ERp18, respectively. Using the known equations for dipolar relaxation (*38*) and the model-free formalism (*28*, *29*), global correlation times, τ_m, were calculated as 9.0 ± 0.4 ns for oxidized ERp18 and 8.0 ± 0.2 ns for reduced ERp18, assuming an average internal motion, τ_e, of 50 ps.

Hydrogen Exchange. Backbone amide ^1H nuclei in retarded exchange with solvent ^2H were identified from rapid HSQC experiments (data not shown). The oxidized protein had 50 unambiguous and a further 5 ambiguous resonances detectable after 510 s, whereas reduced ERp18 had 62 unambiguous and 6 ambiguous resonances detectable after 615 s. Of these, 40 and 42 resonances could be fitted to an exponential decay with a confidence level of over 80% for oxidized and reduced

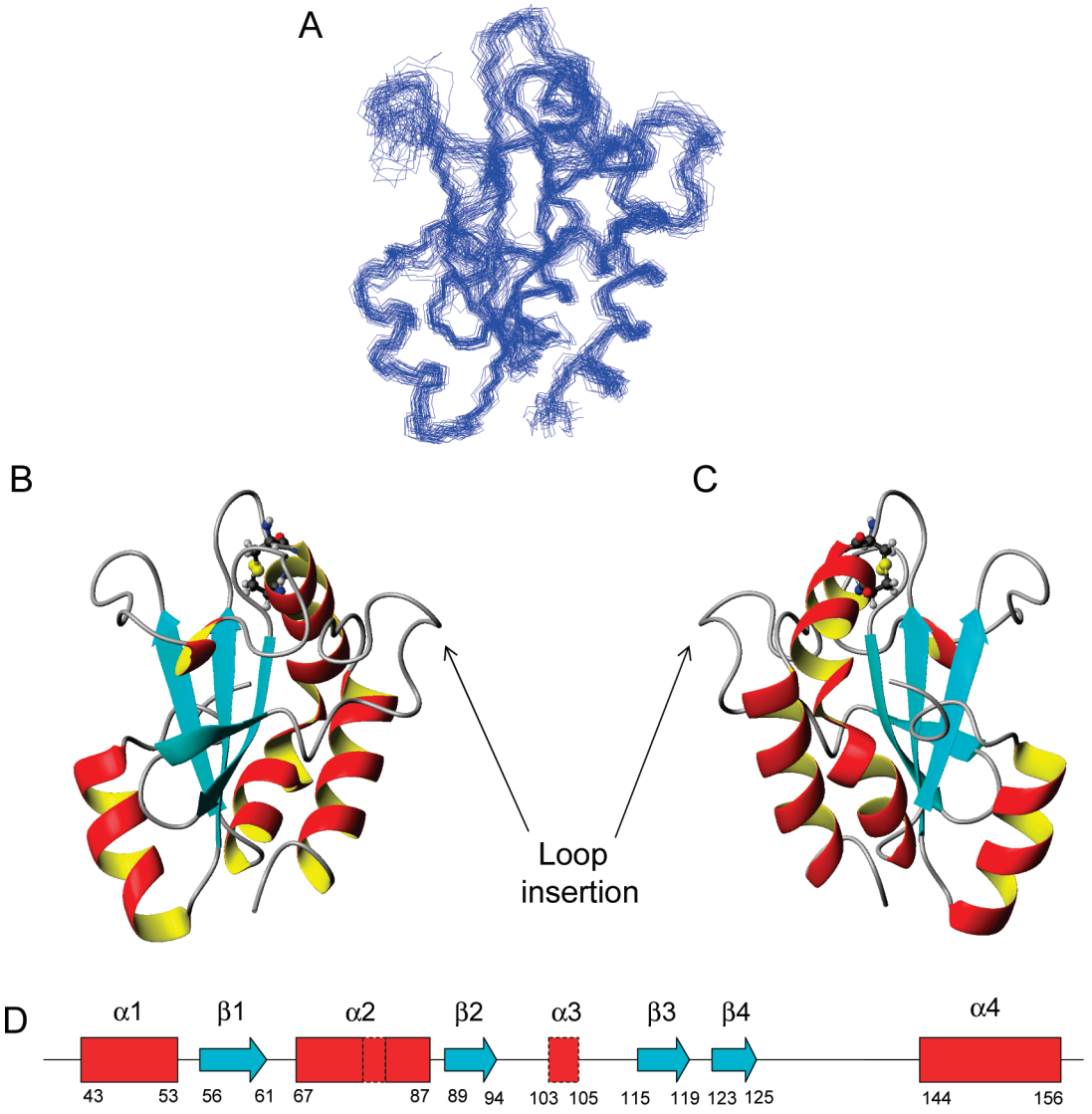

FIGURE 2: Solution structure of oxidized ERp18 showing the 40 structure ensemble with an RMSD over the heavy atoms in secondary structure elements of 0.678 Å (A) and ribbon diagrams of the front (B) and back (C) of the molecule with active site cysteine residues shown by ball and stick representation. The location of secondary structure elements within the sequence is shown with residue numbers beneath (D); blue arrows represent β-strands, red boxes with solid outlines represent α-helices, and red boxes with dashed outlines represent 3_{10}-helices.

ERp18, respectively. Exchange rates were similar for each oxidation state with the exception that residues Trp40 and Lys47 in helix 1, Lys73, Ser83, and Glu84 in helix 2, Gly122 and His125 in strand 4, and Ile128 and Tyr139 in the loop between strand 4 and helix 4 have faster exchange rates in oxidized ERp18 than in reduced ERp18. Ser121 in the loop between strand 3 and strand 4 and Arg157 in the random coil C-terminus showed faster exchange in reduced ERp18.

DISCUSSION

Solution Structure of Oxidized ERp18. The structure reveals a thioredoxin fold with a loop insertion between strand 4 and helix 4 that is adjacent to the active site in the 3D structure (see Figure 2). The position of secondary structure elements within the sequence and therefore the position of the loop are different to those predicted by sequence alignment (*10*), highlighting the necessity of structural studies rather than relying on prediction methods based on sequence alignment. A structure-based sequence alignment between ERp18 and a number of other human thioredoxin-like proteins is shown in Figure 4. The loop insertion is the most noticeable difference in the structure of ERp18 compared to other thioredoxin fold proteins except AGR2 and AGR3. An insertion into the thioredoxin fold is also seen for the bacterial protein DsbA; however, this forms a separate all-helical domain in the loop that contains helix 3 in ERp18, and so is located in a different region of the fold (*39*). This insertion in DsbA is also located in proximity to the active site and is thought to modulate access to it by movement about a hinge region where the two domains join (*40*). From the smaller size and position of the insertion in ERp18 it is unlikely that the loop performs the same function as a large structural change would be needed to prevent access to the N-terminal active site cysteine.

Chemical Shift Differences between Oxidized and Reduced ERp18. Differences in chemical shift between oxidized and reduced ERp18 indicate changes in the electronic environment and hence structural differences. Figure 1C highlights that the largest changes are located in the region of the active site (His62−Lys73). Other residues that show chemical shift differences are Asp96, Glu98, Glu103, Phe105, Ile112, Arg114, and Tyr141. From Figure 5A it is apparent that many of these

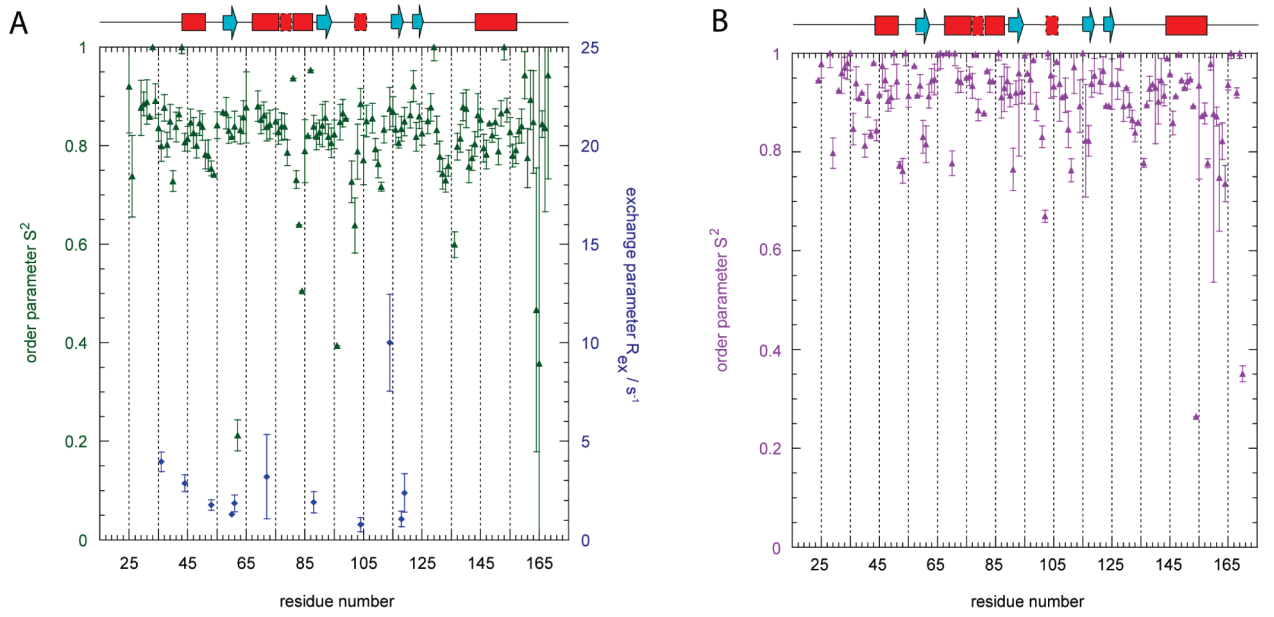

FIGURE 3: Model-free fit parameters for oxidized (A) and reduced (B) ERp18 plotted against residue number. The order parameter S^2 is shown for both oxidized (green) and reduced (purple) ERp18 as solid triangles. The rate of exchange (R_{ex}) is shown as blue diamonds for oxidized ERp18 only. Error bars are the errors obtained directly from the model-free software program. Above each graph is shown a schematic of the secondary structure elements of ERp18 with strands shown as cyan arrows and helices shown as red boxes; boxes with a solid outline denote an α-helix, and boxes with a dotted border denote a 3_{10}-helix.

```
                                                    a       *  *     b                    a
ERp18      SDGHNGLGKGFGDHIHWR-TLEDGKKEAAAS-G--LPLMVIIHKS-WCGACKALKPKFAESTE-ISELSH---NFVMVNL-EDE
Thx        ---------------MVKQIESKTAFQEALDAAG-DKLVVVDFSAT-WCGPCKMIKPFFHSLSEKYS-------NVIFLEVDV-D
PDI_a      --------------DHVLVLRKSNFAEALAA---HKYLLVEFYAP-WCGHCKALAPEYAKAAGKL-KAEGS--EIRLAKVD-AT
PDI_a'     ------------DKQPVKVLVGKNFEDVAFDE--KKNVFVEFYAP-WCGHCKQLAPIWDKLGETY-KDHE---NIVIAKMD-ST
ERp44      -------------------LDTENIDEILNNAD----VALVNFYAD-WCRFSQMLHPIFEEASDVIKEEFPNENQVVFARVD-CD
ERp46_a'   ---------------TVLALTENNFDDTIAEG----ITFIKFYAP-WCGHCKTLAPTWEELSKKEFPGLA---GVKIAEVD-CT
P5_ao      -----AVNGLYSSSDDVIELTPSNFNREVIQS--DSLWLVEFYAP-WCGHCQRLTPEWKKAATAI-KD-----VVKVGAVD-AD
P5_a       ---------------DVIELTDDSFDKNVLDS--EDVWMVEFYAP-WCGHCKNLEPEWAAAASEV-KEQTKG-KVKLAAVD-AT
ERp57_a    --------------SDVLELTDDNFESRISDTGSAGLMLVEFFAP-WCGHCKRLAPEYEAAATRI-----KG-IVPLAKVD-CT
ERp57_a'   -RYLKSEPIPESNDGPVKVVVAENFDEIVNNE--NKDVLIEFYAP-WCGHCKNLEPKYKELGEKLSKDP----NIVIAKMD-AT
ERp72_ao   -----EDDLEVKEENGVLVLNDANFDNFVADK---DTVLLEFYAP-WCGHCKQFAPEYEKIANIL-KD--KDPPIPVAKID-AT
ERP72_a    ---------------VTLVLTKENFDEVVNDA---DIILVEFYAP-WCGHCKKLAPEYEKAAKELSKR---SPPIPLAKVD-AT
ERp72_a'   --------------PVKVVVGKTFDSIVMDP--KKDVLI-EFYAP-WCGHCKQLEPVYNSLAKKY-KGQ-KG--LVIAKMD-AT
TMX        ---------------NVRVITDENWRELL-EG----DWMIEFYAP-WCPACQNLQPEWESFAEWGEDLE-----VNIAKVDV-T
AGR2       ---PQTLSRGWGDDITWVQTYEEALYKSKTSN---KPLMIIHHLDE-CPHSQALKKVFAENKEIQKLAE----QFVLLNLVYET
AGR3       ---HNGLGKGFGDHIHWR-TLE-LFYAQK-SK---KPLMVIHHLED-CQYSQALKKVFAQNEEIQEMAQN---KFIMLNLMHET

                                  c                   d
ERp18      EEPKDEDFSPDGGYIPRILFLDPSG-KVHPEIINENGNPSYKYFYVSAEQVVQGMKEAQERLTGDAFRKKHLEDEL
Thx        DAQDVASEAEVKA-MPTFQFFK-KGQKVGEFS----GA---------NKEKL-EATINELV---------------
PDI_a      EESDLAQQYGVRGY-PTIKFFR-NGDTASPKEYT-AG-R---------EADDIVNWLKKRTGPAA-------------
PDI_a'     AN--EVEAVKVHSF-PTLKFF-PASADRTVIDY--NGER---------TLDGFKKFLESGGQDGAG----------
ERp44      QHSDIAQRYRISKY-PTLKLFR-NGMMMKR-EYR--GQR---------SVKALADYIRQQKSDP------------
ERp46_a'   AERNICSKYSVRGY-PTLLLFR-GGKKVSEHS----GGR---------DLDSLHRFVLSQA-----------KDEL
P5_ao      KHHSLGGQYGVQGF-PTIKIFG-SNKNRPED-YQ--GGR--------TGEAIVDAALSALR---------------
P5_a       VNQVLASRYGIRGF-PTIKIFQ-KGES-PVD-YD--GGR--------TRSDIVSRALDLFSDNA-PPPELLE----
ERp57_a    ANTNTCNKYGVSGY-PTLKIFR-DGEEAG--AYD--GPR--------TADGIVSHLKKQAGPASV-----------
ERp57a'    AN-DVPSPYEVRGF-PTIYFS-PANKKLNPKKYE--GGR--------ELSDFISYLQREAT---------------
ERp72_ao   SASVLASRFDVSGY-PTIKILK---KGQAVD-YE--GSR--------TQEEIVAKVREVSQPDWTPPPEVT-----
ERp72_a    AETDLAKRFDVSGY-PTLKIF---RKGRPYD-Y--NGPR--------EKYGIVDYMIEQSGP--------------
ERp72_a'   ANDVPSDRYKVEGF-PTI-YFAPSGDKKNPVKFE-GGDR--------DLEHLSKF-IEEHATKLSRT-----KEEL
TMX        EQPGLSGRFIITA-LPTI-YHC-KDG--EFRRY--QGPR--------TKKDFINFISDKEWKSIEPVSSWF-----
AGR2       ---TDKHLSPDGQYVPRIMFVDPSL-TVRADITGRYSNRLYAYEPADTALLLDN-MKKALKLL---------KTEL
AGR3       ---TDKNLSPDGQYVPRIMFVDPSL-TVRADIAGRYSNRLYTYEPRDLPLLIEN-MKKALRLI---------QSEL
```

FIGURE 4: Modified sequence alignments of ERp18 with other **a**-like domains of the PDI family. Alignments were modified from initial ClustalW searches to maximize alignment based on equivalent hydrogen bonding between adjacent strands. Secondary structure elements are those defined in the PDB. Strands are shown in cyan, α-helices are shown in red, and 3_{10}-helices are shown in pink. Above the alignment residues of interest have been highlighted: active site motif cysteine residues (or their equivalents) are marked with an "*", residues forming a charge pair thought to be important for proton transfer reactions are marked with an "a", a proline residue found in helix 2 causing it to bend is marked with a "b", the conserved *cis*-proline is marked with a "c", and an arginine residue thought to modulate the pK_a of the C-terminal active site cysteine is marked with a "d".

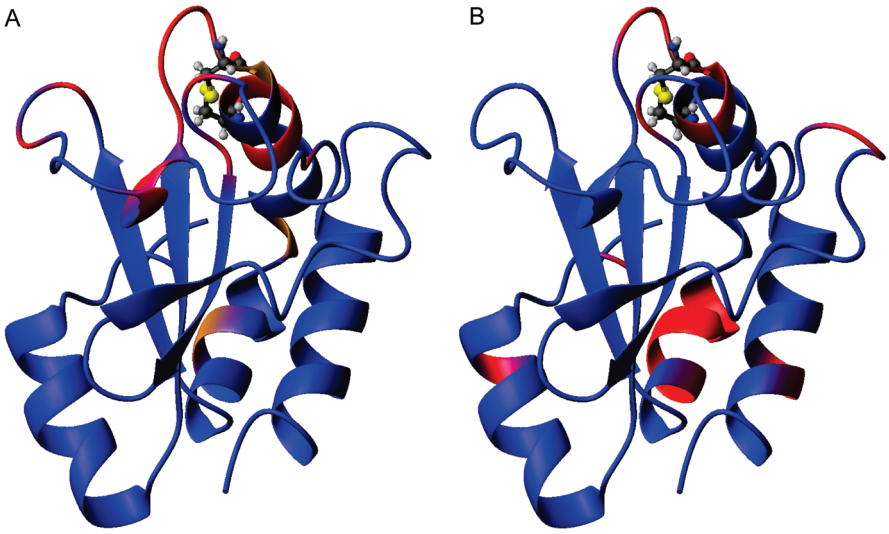

FIGURE 5: Significant differences seen in chemical shifts between oxidized and reduced ERp18 for backbone amide NH and Cα (A) and significant differences seen between the coordinates of the oxidized ERp18 structure and the crystal PDB structure 1SEN with the two structures aligned by the three central strands (B). For (A), red indicates regions where the amide NH chemical shifts reported in Figure 1C are greater than the mean difference; orange indicates Cα shifts greater than the mean plus 2 standard deviations. For (B), red indicates changes in backbone N coordinates between oxidized ERp18 and 1SEN greater than the mean plus 1 standard deviation.

residues are within ~10 Å of the active site region with Asp96 being in the turn immediately after strand 2, Ile112 and Arg114 are on either side of the conserved *cis*-Pro-113 (discussed later) situated at the beginning of strand 3, and Tyr141 is located in the loop preceding helix 4 and is close to the active site. Glu98, Glu103, and Phe90 are further from the active site but may move due to changes in the packing of residues around the upper surface of the molecule.

Structural Comparison with the Unpublished Crystal Structure. The closest structural match to ERp18 was the unpublished crystal structure of Rp19 (1SEN) from the Southeast Collaboratory for Structural Genomics. Rp19 is essentially the same as ERp18 with a different purification tag added during cloning. The crystal structure PDB specifies the presence of a disulfide bond, thus making it the structure of oxidized ERp18 and so both crystal and NMR structures should be almost identical. Two forms of Rp19 are present in the structure file, with the major difference being the presence of two forms of the active site cysteine residues. The disulfide distances for the two forms are 3.77 and 2.38 Å, both values being larger than that expected of a disulfide bond (2.08 Å). Despite no disulfide bond restraints being used in our solution structure calculations, the disulfide distance was found to be 2.03 Å. Close comparison of the NMR structure of ERp18 and the crystal structure Rp19 reveals that the hydrophobic core packing is essentially identical, and the only major difference observed for the region of the active site is that involving the sulfur γ distances as already mentioned. Overlay of the central three β-strands of these two structures gives an RMSD of 0.68 Å for all heavy backbone atoms. The greatest deviations between the two structures are seen in the active site region and in the helix immediately following it as shown in Figure 5B. An RMSD of 2.06 Å is obtained from the overlay of helix 2 alone (Gly67−His87) but the RMSD for the separate N-terminal (Gly67−Pro74) and C-terminal (Lys75−His87) regions of this helix are 0.32 and 1.65 Å, respectively. Interestingly, these areas are seen to display different chemical shift values from our NMR studies of the oxidized and the reduced form of ERp18 and are highlighted in Figure 5A. This suggests that the Rp19 structure is of the reduced protein.

From the PDB header it can be seen that no glutathione was used in the crystallization buffer, and so it is our belief that the crystal structure represents the reduced form of ERp18 rather than the oxidized; this is consistent with the finding that the reduced form is more rigid, and therefore more likely to crystallize, than the more flexible oxidized state. Assuming the crystal structure is indeed that of the reduced form of ERp18, the structures of the two redox states show few differences as seen in other thioredoxin fold proteins such as thioredoxin (*41*) and DsbA (*40*). However, given that currently there is no available report describing the process of obtaining the Rp19 structure, it would be unfair to attempt to extrapolate any further significance between our findings and those pertaining to the Rp19 structure.

Dynamics of Oxidized and Reduced ERp18. Model-free analysis of oxidized and reduced ERp18 (Figure 3) shows similar trends for each oxidation state; in particular, a marked decrease in S^2 can be seen in the loop between β4 and α4 indicating an increased flexibility of this loop. However, a significant difference in the average S^2 values is seen between the two forms, 0.814 ± 0.108 and 0.907 ± 0.101 for oxidized and reduced ERp18, respectively. The higher average S^2 observed for reduced ERp18 indicates a more conformationally rigid structure than that in oxidized ERp18. This is in contrast to dynamics experiments carried out on thioredoxin in which little difference is seen in S^2 between oxidized and reduced forms (*42*). A comparison of NMR ERp18 S^2 values with *B*-factors from 1SEN (Supporting Information) highlights similar regions having motional flexibility and disorder.

Exchange rates of backbone amide hydrogens illustrate that reduced ERp18 forms a more compact structure than that of oxidized ERp18 as more hydrogens are retarded in reduced ERp18 for a longer period of time in D_2O. This increased structural stability is consistent with similar findings using guanidinium chloride denaturation studies of oxidized and reduced ERp18 in which reduced ERp18 remains folded at higher guanidinium chloride concentrations than oxidized ERp18 (*10*). This difference in structural stability emphasizes that the disulfide bond formed in ERp18 is functional and not structural as in many other proteins.

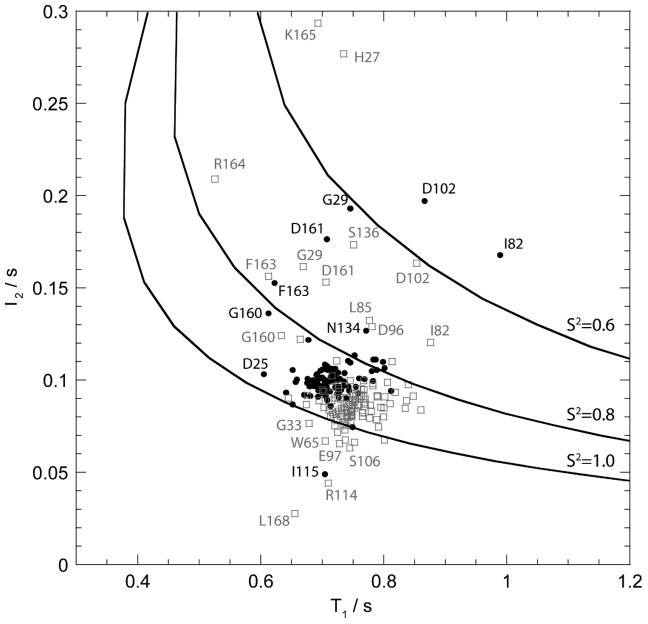

FIGURE 6: Plot of experimental T_1 against T_2 for each amide $^1H-^{15}N$ of oxidized (□) and reduced (●) ERp18. Contour lines are calculated using the spectral density function from the model-free formalism for the order parameter S^2 = 0.6, 0.8, and 1.0. Residues that fall away from the clustered majority are labeled with residue type and number.

Figure 6 shows a plot of T_2 against T_1 for each amide ^{15}N in oxidized and reduced ERp18. The contours represent the model-free S^2 parameter with values of 0.6, 0.8, and 1.0 and constant τ_e of 50 ps. The plot shows that the data for the oxidized form of ERp18 are more dispersed while the data for reduced ERp18 form a more compact cluster indicating a more uniform behavior in reduced ERp18. In this plot, residues that have an S^2 value of less than 0.8 show increased motion in the pico- to nanosecond time scale indicating increased flexibility and are confirmed by the heteronuclear NOE experiments. These motions are observed in both oxidation states of ERp18 and are restricted mainly to residues in loops located close to the active site in the 3D structure and in the helix immediately following it. Residues that have an S^2 value greater than 1.0 (1.0 denotes fully rigid structure) are residues that have short T_2 values indicating line broadening caused by exchange and milli- to microsecond motion and are also mainly located in loops around the active site region. Residues that fall into this second category are predominantly from oxidized ERp18. This finding is in agreement with model-free analysis where R_{ex} values were only required to fit oxidized data. Relaxation analysis highlights that only oxidized ERp18 displays motion in the milli- to microsecond time scale, and so conformational exchange is limited to this oxidation state of the protein. Residues found to be in conformational exchange were found to be predominantly located in the helix immediately following the active site and those regions in close structural proximity to this helix.

The calculated global correlation times, τ_m, were 9.0 ± 0.4 ns for oxidized ERp18 and 8.0 ± 0.2 ns for reduced ERp18, suggesting once again a more compact structure for the reduced form of ERp18. For *E. coli* thioredoxin, τ_m values were found to be 6.41 ± 0.04 ns for oxidized thioredoxin and 6.30 ± 0.01 ns for reduced thioredoxin (*42*), reflecting not only the smaller size of the thioredoxin molecule (~12 kDa) but also the high degree of similarity between the two forms. In contrast to this, the τ_m values for the thioredoxin-like domain of the *E. coli* protein DsbA are 12.70 and 10.73 ns for oxidized and reduced DsbA, respectively (*40*). In addition, greater levels of exchange are seen in oxidized DsbA as in ERp18. DsbA is a known oxidase enzyme, and the dynamics reflect this in that a shorter τ_m and lower levels of exchange for the reduced form suggest a higher structural stability; DsbA would therefore adopt the reduced conformation in preference to the oxidized and in turn oxidize other molecules or substrates. Our relaxation dynamics therefore indicate that ERp18 is also an oxidase and will preferentially adopt the reduced form over substrate molecules as indicated by the shorter global correlation time in reduced ERp18.

The τ_m of a 132-residue protein molecule can be estimated as 9.59 ns at 25 °C using equations by Daragon and Mayo (*43*); this discounts approximately 25 residues at the termini of ERp18 that are unstructured, as determined from both the lack of NOE contacts and fast picosecond motion observed in the heteronuclear NOE data for both oxidation states of ERp18. The τ_m values for ERp18 are indicative of a monomer in solution, in contrast to that reported by Jeong et al. (*13*), who saw a dimer: a larger τ_m would be expected for a larger entity. Our observation of a monomer is further confirmed from the collection of TOCSY-based NMR data for ERp18 which would not have been possible for a species with a molecular mass in excess of approximately 20 kDa.

Presence of Conserved Features Found in Human PDI-like Domains. The highly conserved *cis*-proline peptide bond within thioredoxin family members has importance for the activity of these oxidoreductases. Chemical shift assignments and structure calculations confirm that proline-113 is in the *cis* conformation in ERp18 and is situated in a loop adjacent to the active site at the C-terminus of the antiparallel β-strand. The crystal structure of ERp18 (1SEN) also shows the conformation of proline-113 to be in the *cis* rather than *trans* conformation.

The presence of the second conserved proline residue, the one found in helix 2, causes this helix to bend. The bend in oxidized ERp18 is almost 90°, more than that seen in other PDI family members. Proline residues cause bends in helices because of the disruption in hydrogen bonding caused by the lack of an amide proton (*44*); this in turn gives the helix increased flexibility as is seen by decreased S^2 values for this region of the protein. The highly conserved nature of this proline residue and the scarcity of this residue in helices suggest an important functional role for this feature;, however, this function has not yet been elucidated for any family member.

The charged pair of residues seen in thioredoxin and PDI **a** and **a**′ domains that are thought to be involved in structural stability and proton transfer reactions during disulfide bond isomerization (*6*−*8*) are located on the central β-sheet with the side chains protruding toward the active site. The sequence alignment in Figure 4 shows the equivalent residues to Glu30 and Lys64 in PDI **a** to be Ile60 and Asn93 which do not exist as charged species at physiological pH. As this charge pair is believed to be important in thioredoxin-like species, it is expected that ERp18 will possess equivalent residues. Inspection of the charged residues in the vicinity of the active site in ERp18 reveal His62 and Glu95 to be potential candidates for performing the role played by these charged residues. These residues are as much as 2 Å closer to the active site cysteine sulfur atoms than the charged residues Glu30 and Lys64 found in the **a** domain of PDI and are capable of forming a salt bridge and so are likely to be

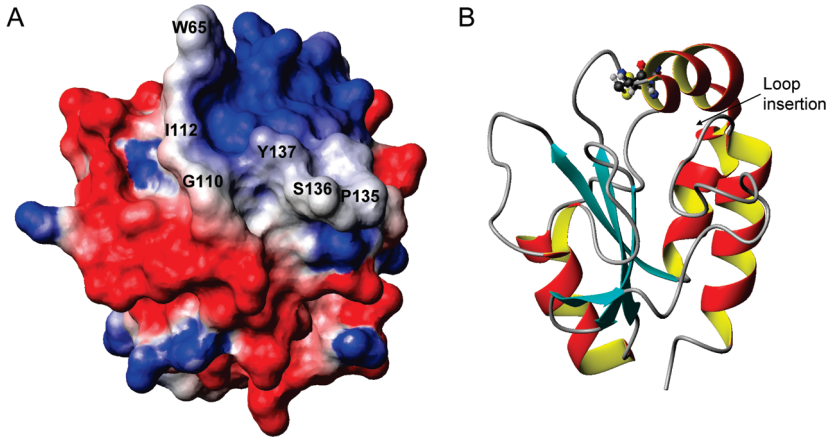

FIGURE 7: Potential binding site of ERp18. Surface charge potential diagram (A) and ribbon representation in the same orientation (B) of oxidized ERp18. In (A), the blue coloration represents positively charged areas, red represents negatively charged areas, and gray represents neutral (hydrophobic) areas. Key residues that are speculated to be involved in substrate binding are labeled. The figure was generated using default parameters in MOLMOL (*48*).

capable of performing the same function. However, it is unclear why the amino acid type and position of these conserved charged residues are different in ERp18 than in other human PDI family members.

The sequence alignment in Figure 4 shows that there is no arginine residue present anywhere in the loop preceding helix 4 as is the case in all other PDI family members, and this conserved arginine is considered to play an important role in the PDI catalytic cycle (*9*). In ERp18, this loop contains 11 inserted residues compared to PDI itself and was found by NMR relaxation dynamics to have increased flexibility in both oxidized and reduced ERp18 as shown by lower S^2 values (Figure 3). This insertion is shared only by the AGR2 and AGR3 molecules which, according to the alignment, do contain an arginine residue within this loop. Unfortunately, there is currently no structure published for either AGR protein nor have any detailed mechanistic studies been reported, and so it cannot be confirmed that this arginine residue is the equivalent to Arg103 in PDI **a**. The designation of an equivalent residue is also complicated by the sequence alignment being somewhat ambiguous in this area and a second arginine residue that could also be a potential candidate for this role.

The solution structure of ERp18 can be used to propose a potential equivalent residue to Arg103 from PDI **a**, and close inspection of the orientation of the side chains of residues in this loop for each structure in the oxidized ERp18 NMR ensemble has revealed that the distance between Sγ of Cys69 and Oη of Tyr141 varies from 5.0 to 16.4 Å. This is not seen for any of the other residues in this loop and so has potential to be a significant feature of Tyr141. This behavior within the ensemble was used to identify Arg103 in PDI **a** (*9*). There is the possibility that the side chain of Tyr141 could modify the pK_a of the active site cysteines in ERp18 by stabilizing the thiolate anion in conjunction with acid−base assistance from His62 and Glu95 (the charged residues situated close to the active site cysteines), but there is no evidence from biochemistry or mutagenesis that this the case. However, it was reported by Alanen et al. (*10*) that the rate-limiting step of ERp18-catalyzed oxidation was the oxidation of the substrate in contrast to other PDI family members where the rate-limiting step is reoxidation of the enzyme. As Arg103 in PDI **a** is thought to be an important factor in the mechanism of substrate oxidation versus enzyme reoxidation by modulating the pK_a of the C-terminal active site cysteine (*9*), it is possible that the difference in the comparative rates of these reactions in ERp18 is due to the equivalent role being carried out by this putative tyrosine residue.

The loop preceding helix 4, being unique to ERp18, AGR2, and AGR3, may have functional significance as it contains a number of hydrophobic residues that define an extended hydrophobic patch adjacent to the active site, as seen in Figure 7, and so could potentially be involved in substrate binding. This region of the structure is comparable to a hydrophobic surface seen in *E. coli* thioredoxin (*45*), and residues in this region also show significant backbone chemical shift differences between oxidized and reduced thioredoxin species (*41*), as seen in Figure 1 for equivalent areas in ERp18. Furthermore, Qin et al. have determined the structures of mixed disulfides of human thioredoxin with target peptides from the transcription factor NFκB (*46*) and ref-1 (*47*), again showing that hydrophobic residues in comparable loops close to the active site in the thioredoxin structure are involved in substrate binding.

This study has highlighted the difference in the conformational rigidity of oxidized and reduced ERp18, with both relaxation dynamics and hydrogen exchange experiments showing that reduced ERp18 forms a more compact structure. This property suggests that the function of ERp18 is to oxidize disulfide bonds in substrates, and in doing so it will itself become reduced and more stable. The relaxation analysis has also uncovered the highly flexible nature of the unique loop situated between strand 4 and helix 4 and in close proximity to the active site in the 3D structure.

Further studies involving site-directed mutagenesis will confirm the importance of residues identified in this study and how they are implicated in the reaction mechanism of ERp18. Although no natural substrates of ERp18 are known, finding molecules that bind to ERp18 is also key in helping to understand its function in more detail and could help unravel the mechanism of thiol−disulfide exchange reactions involved in the production of nascent secretory proteins.

SUPPORTING INFORMATION AVAILABLE

Top 50 structural matches using Dali; T_1, T_2, and heteronuclear NOE plots for oxidized and reduced ERp18; graph of the difference in hydrogen exchange rates between oxidized and reduced ERp18; plot of *B*-factors from 1SEN. This material is available free of charge via the Internet at http://pubs.acs.org.

REFERENCES

1. Appenzeller-Herzog, C., and Ellgaard, L. (2008) The human PDI family: versatility packed into a single fold. *Biochim. Biophys. Acta 1783*, 535–548.
2. Ellgaard, L., and Ruddock, L. W. (2005) The human protein disulphide isomerase family: substrate interactions and functional properties. *EMBO Rep. 6*, 28–32.
3. Charbonnier, J. B., Belin, P., Moutiez, M., Stura, E. A., and Quemeneur, E. (1999) On the role of the cis-proline residue in the active site of DsbA. *Protein Sci. 8*, 96–105.
4. Tian, G., Xiang, S., Noiva, R., Lennarz, W. J., and Schindelin, H. (2006) The crystal structure of yeast protein disulfide isomerase suggests cooperativity between its active sites. *Cell 124*, 61–73.
5. Vitu, E., Gross, E., Greenblatt, H. M., Sevier, C. S., Kaiser, C. A., and Fass, D. (2008) Yeast Mpd1p reveals the structural diversity of the protein disulfide isomerase family. *J. Mol. Biol. 384*, 631–640.
6. Kemmink, J., Darby, N. J., Dijkstra, K., Nilges, M., and Creighton, T. E. (1996) Structure determination of the N-terminal thioredoxin-like domain of protein disulfide isomerase using multidimensional heteronuclear $^{13}C/^{15}N$ NMR spectroscopy. *Biochemistry 35* 7684–7691.
7. Langsetmo, K., Fuchs, J. A., and Woodward, C. (1991) The conserved, buried aspartic acid in oxidized *Escherichia coli* thioredoxin has a pK_a of 7.5. Its titration produces a related shift in global stability. *Biochemistry 30*, 7603–7609.
8. Langsetmo, K., Fuchs, J. A., Woodward, C., and Sharp, K. A. (1991) Linkage of thioredoxin stability to titration of ionizable groups with perturbed pK_a. *Biochemistry 30*, 7609–7614.
9. Lappi, A. K., Lensink, M. F., Alanen, H. I., Salo, K. E., Lobell, M., Juffer, A. H., and Ruddock, L. W. (2004) A conserved arginine plays a role in the catalytic cycle of the protein disulphide isomerases. *J. Mol. Biol. 335*, 283–295.
10. Alanen, H. I., Williamson, R. A., Howard, M. J., Lappi, A.-K., Jantti, H. P., Rautio, S. M., Kellokumpu, S., and Ruddock, L. W. (2003) Functional characterization of ERp18, a new endoplasmic reticulum-located thioredoxin superfamily member. *J. Biol. Chem. 278*, 28912–28920.
11. Knoblach, B., Keller, B. O., Groenendyk, J., Aldred, S., Zheng, J., Lemire, B. D., Li, L., and Michalak, M. (2003) ERp19 and ERp46, new members of the thioredoxin family of endoplasmic reticulum proteins. *Mol. Cell Proteomics 2*, 1104–1119.
12. Liu, F., Rong, Y. P., Zeng, L. C., Zhang, X., and Han, Z. G. (2003) Isolation and characterization of a novel human thioredoxin-like gene hTLP19 encoding a secretory protein. *Gene 315*, 71–78.
13. Jeong, W., Lee, D. Y., Park, S., and Rhee, S. G. (2008) ERp16, an endoplasmic reticulum-resident thiol-disulfide oxidoreductase: biochemical properties and role in apoptosis induced by endoplasmic reticulum stress. *J. Biol. Chem. 283*, 25557–25566.
14. Wishart, D. S., and Sykes, B. D. (1994) Chemical shifts as a tool for structure determination. *Methods Enzymol. 239*, 363–392.
15. Piotto, M., Saudek, V., and Sklenar, V. (1992) Gradient-tailored excitation for single-quantum NMR spectroscopy of aqueous solutions. *J. Biomol. NMR 2*, 661–665.
16. States, D. J., Haberkorn, R. A., and Ruben, D. J. (1982) A two-dimensional nuclear Overhauser experiment with pure absorption phase in 4 quadrants. *J. Magn. Reson. 48*, 286–292.
17. Delaglio, F., Grzesiek, S., Vuister, G. W., Zhu, G., Pfeifer, J., and Bax, A. (1995) *J. Biomol. NMR 6*, 277–293.
18. Johnson, B. A., and Blevins, R. A. (1994) NMR view—a computer program for the visualization and analysis of NMR data. *J. Biomol. NMR 4*, 603–614.
19. Johnson, B. A. (2004) Using NMRView to visualize and analyze the NMR spectra of macromolecules. *Methods Mol. Biol. 278* 313–352.
20. Fogh, R., Ionides, J., Ulrich, E., Boucher, W., Vranken, W., Linge, J. P., Habeck, M., Rieping, W., Bhat, T. N., Westbrook, J., Henrick, K., Gilliland, G., Berman, H., Thornton, J., Nilges, M., Markley, J., and Laue, E. (2002) The CCPN project: an interim report on a data model for the NMR community. *Nat. Struct. Biol. 9*, 416–418.
21. Vranken, W. F., Boucher, W., Stevens, T. J., Fogh, R. H., Pajon, A., Llinas, M., Ulrich, E. L., Markley, J. L., Ionides, J., and Laue, E. D. (2005) The CCPN data model for NMR spectroscopy: development of a software pipeline. *Proteins 59*, 687–696.
22. Brunger, A. T., Adams, P. D., Clore, G. M., DeLano, W. L., Gros, P., Grosse-Kunstleve, R. W., Jiang, J. S., Kuszewski, J., Nilges, M., Pannu, N. S., Read, R. J., Rice, L. M., Simonson, T., and Warren, G. L. (1998) Crystallography & NMR system: a new software suite for macromolecular structure determination. *Acta Crystallogr., Sect. D: Biol. Crystallogr. 54*(Part 5), 905–921.
23. Cornilescu, G., Delaglio, F., and Bax, A. (1999) Protein backbone angle restraints from searching a database for chemical shift and sequence homology. *J. Biomol. NMR 13*, 289–302.
24. Fossi, M., Oschkinat, H., Nilges, M., and Ball, L. J. (2005) Quantitative study of the effects of chemical shift tolerances and rates of SA cooling on structure calculation from automatically assigned NOE data. *J. Magn. Reson. 175*, 92.
25. Barbato, G., Ikura, M., Kay, L. E., Pastor, R. W., and Bax, A. (1992) Backbone dynamics of calmodulin studied by ^{15}N relaxation using inverse detected two-dimensional NMR spectroscopy: the central helix is flexible. *Biochemistry 31*, 5269–5278.
26. Neuhaus, D., and Vanmierlo, C. P. M. (1992) Measurement of heteronuclear noe enhancements in biological macromolecules—a convenient pulse sequence for use with aqueous solutions. *J. Magn. Reson. 100*, 221–228.
27. Noggle, J. H., and Schirmer, R. E. ((1971)) *The Nuclear Overhauser Effect: Chemical Applications*, Academic Press, New York..
28. Lipari, G., and Szabo, A. (1982) Model-free approach to the interpretation of nuclear magnetic resonance relaxation in macromolecules. 1. Theory and range of validity. *J. Am. Chem. Soc. 104* 4546–4559.
29. Lipari, G., and Szabo, A. (1982) Model-free approach to the interpretation of nuclear magnetic resonance relaxation in macromolecules. 2. Analysis of experimental results. *J. Am. Chem. Soc. 104*, 4559–4570.
30. Palmer, A. G., Rance, M., and Wright, P. E. (1991) Intramolecular motions of a zinc finger DNA-binding domain from Xfin characterized by proton-detected natural abundance C-12 heteronuclear NMR spectroscopy. *J. Am. Chem. Soc. 113*, 4371–4380.
31. Howarth, O. W., and Lilley, D. M. J. (1978) Carbon-13 NMR of peptides and proteins. *Prog. Nucl. Magn. Reson. Spectrosc. 12*, 1–40.
32. van Gunsteren, W. F., Brunne, R. M., Gros, P., van Schaik, R. C., Schiffer, C. A., and Torda, A. E. (1994) Accounting for molecular mobility in structure determination based on nuclear magnetic resonance spectroscopic and X-ray diffraction data. *Methods Enzymol. 239*, 619–654.
33. Guex, N., and Peitsch, M. C. (1997) SWISS-MODEL and the Swiss-PdbViewer: an environment for comparative protein modeling. *Electrophoresis 18*, 2714–2723.
34. Laskowski, R. A., Rullmannn, J. A., MacArthur, M. W., Kaptein, R., and Thornton, J. M. (1996) AQUA and PROCHECK-NMR: programs for checking the quality of protein structures solved by NMR. *J. Biomol. NMR 8*, 477–486.
35. Holm, L., and Sander, C. (1996) Mapping the protein universe. *Science 273*, 595–603.
36. Stirnimann, C. U., Rozhkova, A., Grauschopf, U., Bockmann, R. A., Glockshuber, R., Capitani, G., and Grutter, M. G. (2006) High-resolution structures of *Escherichia coli* cDsbD in different redox states: a combined crystallographic, biochemical and computational study. *J. Mol. Biol. 358*, 829–845.
37. Zhang, Y. Z., Cheng, H., Gould, K. L., Golemis, E. A., and Roder, H. (2003) Structure, stability, and function of hDim1 investigated by NMR, circular dichroism, and mutational analysis. *Biochemistry 42*, 9609–9618.
38. Farrow, N. A., Zhang, O., Szabo, A., Torchia, D. A., and Kay, L. E. (1995) Spectral density function mapping using ^{15}N relaxation data exclusively. *J. Biomol. NMR 6*, 153–162.
39. Martin, J. L., Bardwell, J. C., and Kuriyan, J. (1993) Crystal structure of the DsbA protein required for disulphide bond formation in vivo. *Nature (London) 365*, 464–468.
40. Horne, J., d'Auvergne, E. J., Coles, M., Velkov, T., Chin, Y., Charman, W. N., Prankerd, R., Gooley, P. R., and Scanlon, M. J. (2007) Probing the flexibility of the DsbA oxidoreductase from Vibrio cholerae—a $^{15}N-^{1}H$ heteronuclear NMR relaxation analysis of oxidized and reduced forms of DsbA. *J. Mol. Biol. 371*, 703–716.
41. Dyson, H. J., Holmgren, A., and Wright, P. E. (1988) Structural differences between oxidised and reduced thioredoxin monitored by two-dimensional ^{1}H NMR spectroscopy. *Eur. J. Biochem. 228* 254–258.
42. Stone, M. J., Chandrasekhar, K., Holmgren, A., Wright, P. E., and Dyson, H. J. (1993) Comparison of backbone and tryptophan side-chain dynamics of reduced and oxidized *Escherichia coli* thioredoxin using ^{15}N NMR relaxation measurements. *Biochemistry 32*, 426–435.
43. Daragan, V. A., and Mayo, K. H. (1997) Motional model analyses of protein and peptide dynamics using ^{13}C and ^{15}N NMR relaxation. *Prog. Nucl. Magn. Reson. Spectrosc. 31*, 63–105.
44. Barlow, D. J., and Thornton, J. M. (1988) Helix geometry in proteins. *J. Mol. Biol. 201*, 601–619.

45. Eklund, H., Cambillau, C., Sjoberg, B. M., Holmgren, A., Jornvall, H., Hoog, J. O., and Branden, C. I. (1984) Conformational and functional similarities between glutaredoxin and thioredoxins. *EMBO J. 3*, 1443–1449.
46. Qin, J., Clore, G. M., Kennedy, W. M., Huth, J. R., and Gronenborn, A. M. (1995) Solution structure of human thioredoxin in a mixed disulfide intermediate complex with its target peptide from the transcription factor NF kappa B. *Structure 3*, 289–297.
47. Qin, J., Clore, G. M., Kennedy, W. P., Kuszewski, J., and Gronenborn, A. M. (1996) The solution structure of human thioredoxin complexed with its target from Ref-1 reveals peptide chain reversal. *Structure 4*, 613–620.
48. Koradi, R., Billeter, M., and Wuthrich, K. (1996) MOLMOL: a program for display and analysis of macromolecular structures. *J. Mol. Graphics 14*, 29–32.